# Determination of Oxygen Nonstoichiometry and Diffusivity in Mixed Conducting Oxides by Oxygen Coulometric Titration

## I. Chemical Diffusion in $La_{0.8}Sr_{0.2}CoO_{3-\delta}$

**M. H. R. Lankhorst and H. J. M. Bouwmeester**

*Laboratory for Inorganic Materials Science, Department of Chemical Technology, University of Twente, 7500 AE Enschede, The Netherlands*

ABSTRACT

Oxygen coulometric titration has been applied to measure chemical diffusion in $La_{0.8}Sr_{0.2}CoO_{3-\delta}$ between 700 and 1000°C. The transient current response to a potentiostatic step has been transformed from the time domain to the frequency domain. The equivalent circuit used to fit the resulting impedance data contains the element that describes the finite-length diffusion of oxygen into the sample specimen. Other elements included are the gas-phase capacitance and the sum of the gas-phase diffusion resistance and that associated with the limited surface exchange kinetics of the sample. The chemical diffusion coefficient of perovskite $La_{0.8}Sr_{0.2}CoO_{3-\delta}$ has been determined as a function of temperature and oxygen partial pressure. Its value can be represented by $\tilde{D}$ (cm²/s) = 5.91 × exp [(−135 kJ/mol)/$RT$], and turns out to be practically independent of oxygen partial pressure in the range $10^{-2}$ − 0.209 bar.

### Introduction

Mixed ionic and electronic conducting perovskites $La_{1-x}Sr_xCoO_{3-\delta}$ receive wide attention to date because of their potential applications as gas separation membranes, oxidation catalysts, and as electrodes in solid oxide fuel cells and oxygen sensors. High ionic conductivity in these materials at elevated temperatures results from large oxygen vacancy concentration in conjunction with a high vacancy diffusivity. Although the ionic transference number remains below a value of 0.01, the ionic conductivity may be one to two orders of magnitude higher than that of stabilized zirconia. An obvious consideration to the design of the aforementioned applications is to know how these parameters depend on environmental parameters like oxygen partial pressure and temperature.

Changes in the oxygen vacancy concentration as a function of temperature and oxygen partial pressure are commonly measured using thermogravimetry or coulometric titration. An advantage of the latter technique is that electrical currents and voltages can be measured with high accuracy. An additional advantage is that coulometric titration permits direct control of the oxygen stoichiometry of the sample specimen, which allows easy determination of thermodynamic quantities such as the partial energy and entropy associated with oxygen incorporation into the oxide.[1,2] Chemical diffusion coefficients can be measured simultaneously by monitoring the rate at which the electrochemical cell proceeds to equilibrium after the cell is imposed to a sudden change in either the voltage or the current. Thus obtained chemical diffusion coefficients can be used to calculate the corresponding vacancy diffusion coefficients when combined with equilibrium data of the oxygen stoichiometry as a function of oxygen partial pressure.

The value of the vacancy diffusion coefficient can also be obtained from data of the ionic conductivity. However, the direct measurement of ionic conductivity in predominant electronically conducting oxides is often complicated due to short-circuiting paths for oxygen transport, such as diffusion of oxygen species along the oxide surface or via the gas phase through rapid exchange. This leads to overestimates of the ionic conductivity.[3] Another problem is the possibility of an interfacial reaction between the oxide and the blocking electrode material or the glass used for sealing to suppress parasitic contributions to oxygen transport. Also, the ionic conductivity can be determined from steady-state oxygen permeation experiments, assuming negligible influence of the oxygen exchange kinetics at the gas solid interface.[4] It may be noted that such an assumption is not required when using coulometric titration. Since the time dependence of bulk diffusion differs from that of the surface exchange kinetics, these can be distinguished by analysis of the experimental data in the frequency domain.

In this paper, the oxygen nonstoichiometry and diffusivity of perovskite $La_{0.8}Sr_{0.2}CoO_{3-\delta}$ are measured by oxygen coulometric titration. The chemical diffusion coefficient is determined from analysis of the transient current response to potentiostatic steps. Oxygen nonstoichiometry data which includes determination of the partial energy and entropy associated with oxygen incorporation are presented in Part II of this paper.[5]

### Theory

*Chemical diffusion.*—When an oxygen chemical potential gradient is present in the bulk of a mixed oxygen ion and electron conducting oxide, oxygen ions diffuse in the direction toward low oxygen chemical potential. The oxygen flux $J_0$ is related to the gradient in oxygen chemical potential $\mu_{O_2}$ as given by the Wagner equation [6,7]

$$J_o = -\frac{1}{8F^2}\sigma_o t_e \nabla \mu_{O_2} \quad [1]$$

where $\sigma_0$ is the conductivity of oxygen ions, $t_e$ the electron transference number, and $F$ Faraday's constant. Perovskites $La_{1-x}Sr_xCoO_{3-\delta}$ show predominantly electronic conduction so that $t_e$ takes a value of unity. To describe the case of nonsteady state transport of oxygen, Eq. 1 is commonly rewritten in terms of the oxygen concentration gradient $\nabla c_O$

$$J_o = -\tilde{D}\nabla c_o \quad [2]$$

where $\tilde{D}$ is the chemical diffusion coefficient. It follows that ($t_e = 1$)

$$\tilde{D} = \frac{\sigma_o}{8F^2}\left(\frac{\partial \mu_{O_2}}{\partial c_O}\right) \quad [3]$$

where the term between parenthesis can be obtained independently by measuring the oxygen stoichiometry of the sample as a function of its equilibrium oxygen chemical potential. Combining Eq. 3 with Nernst-Einstein

$$\sigma_O = \frac{D_O c_O 4F^2}{RT} \quad [4]$$

where $R$ is the gas constant, $T$ the temperature, and $D_O$ the oxygen self-diffusion coefficient, leads to the following relationship between the chemical diffusion coefficient $\tilde{D}$ and $D_O$

$$\tilde{D} = D_{O}\left(\frac{1}{2}\frac{\partial \ln P_{O_2}}{\partial \ln c_{O}}\right) \quad [5]$$

where $P_{O_2}$ is the oxygen partial pressure. Oxygen ion movement through the perovskite lattice is assumed to occur via a hopping process over vacant oxygen sites. If it is further assumed that all these vacancies are equivalent, one may derive

$$\tilde{D} = D_{V}\left(-\frac{1}{2}\frac{\partial \ln P_{O_2}}{\partial \ln c_{V}}\right) \quad [6]$$

where $c_V$ is the concentration of oxygen vacancies with diffusion coefficient $D_V$. The terms between parentheses in Eq. 5 and 6 are referred to as thermodynamic factors.

*Coulometric titration.*—In a high-temperature oxygen coulometric titration setup the sample is enclosed in a sealed compartment. Using $P_{O_2}^{ref}$ and $P_{O_2}^{cell}$ to denote the respective oxygen partial pressures of the reference gas and that of the gas inside the compartment, the experimental arrangement can be represented as

$$P_{O_2}^{ref.}, Pt|YSZ^{I}|Pt, P_{O_2}^{cell}, La_{0.8}Sr_{0.2}CoO_{3-\delta}, Pt|YSZ^{EMF}|Pt, P_{O_2}^{ref} \quad [7]$$

Two zirconia electrolyte cells are used. The first, given at the left-hand of Eq. 7, is used to adjust the oxygen stoichiometry of the sample by electrochemically pumping oxygen into or out of the enclosure. The electromotive force (*EMF*) measured across the second cell, denoted as $YSZ^{EMF}$, is given by

$$EMF = \frac{RT}{4F}\ln\left(\frac{P_{O_2}^{ref}}{P_{O_2}^{cell}}\right) \quad [8]$$

The electric current $I$ passing through $YSZ^{I}$ can be related to the stoichiometry change of the sample specimen. In practice, one also needs to consider the concomitant change of the oxygen concentration in the gas phase.

In general, oxygen coulometric titration measurements can be performed either by monitoring the *EMF* response to a dc current pulse of known duration (galvanostatic method[8]) or by monitoring the current decay after a stepwise change in the *EMF* (potentiostatic method[9,10]). In view of Eq. 8, a potentiostatic step involves a change in oxygen partial pressure inside the cell. Chemical diffusion allows the sample to adapt its stoichiometry to the newly adjusted $P_{O_2}^{cell}$. The rate of equilibration is monitored by measuring the current, which decays over time toward a minimum value. The latter is due to the unavoidable leakage current and is determined by the quality of the glass sealing, and the nonvanishing electronic conductivity of the zirconia electrolyte.

For nonstoichiometric oxides, application of the potentiostatic over the galvanostatic step method has some advantages, which include: (*i*) easy determination of the leakage current, toward which the current decays after a potentiostatic step; and (*ii*) at the end of the current decay, the cell is in a steady state because $P_{O_2}^{cell}$ is fixed by the imposed *EMF*. On the contrary, at the end of a galvanostatic pulse, the oxygen partial pressure drifts back to that of the ambient value by leakage of oxygen.

During a galvanostatic pulse of finite duration, the ohmic IR-drop does not affect the voltage decay, and is merely superimposed as a constant. In the potentiostatic step method the IR-drop is time dependent, which complicates analysis of the decay current in the time domain. The analysis can, however, still be carried out by transforming the experimental data to the frequency domain.

*Analysis of the experimental decay current.*—The transient current response to a voltage step is commonly analyzed by fitting the current to a $t^{-1/2}$ behavior for short times and to an $\exp(-t/\tau)$ behavior for long times.[9,11] Both the short and longtime approximation are based on the assumption that the magnitude and the time dependence of the decay current are determined solely by chemical diffusion of oxygen inside the oxide. In general, however, the decay current may also be affected by gas-phase diffusion inside the cell, limited oxygen exchange kinetics across the oxide surface, and polarization losses over the electrical wiring and contacts. These contributions may be discriminated from chemical diffusion when the time constants characteristic of these processes differ from that of chemical diffusion. A possible route is the direct measurement of the cell-impedance using frequency response techniques, but these are very time consuming if measurements have to be performed at low frequencies. It is also possible to obtain the cell-impedance as a function of frequency by Fourier transformation of the transient current response. The resulting impedance data can be fitted to an equivalent circuit that includes, among others, the element which describes diffusion in the oxide.

An expression for the impedance element associated with chemical diffusion of oxygen can be obtained by solving Fick's second law under the appropriate boundary conditions. For a sample of thickness $L$ and radius $R$, Fick's second law in cylindrical coordinates $(x, r)$ reads

$$\frac{\partial c_{O}(x, r, t)}{\partial t} = \tilde{D}\left(\frac{\partial^2 c_{O}(x, r, t)}{\partial x^2} + \frac{\partial^2 c_{O}(x, r, t)}{\partial r^2} + \frac{1}{r}\frac{\partial c_{O}(x, r, t)}{\partial r}\right) \quad [9]$$

If the equilibrium oxygen concentration changes from $c_O^0$ to $c_O^\infty$ as a result of the change in $P_{O_2}^{cell}$, the following boundary conditions apply

$$c_{O}(x, r, t = 0) = c_{O}^{0} \quad [10]$$

$$c(x = -1/2L, r, t) = c(x = 1/2L, r, t) = c(x, r = R, t) = c_{O}^{\infty} \quad [11]$$

$$\frac{\partial c_{O}(x, r = 0, t)}{\partial r} = 0 \quad [12]$$

The solution is given by

$$c_{O} = c_{O}^{\infty} - \left(c_{O}^{\infty} - c_{O}^{\infty}\right)\sum_{i\in N^+}\sum_{n\in N^+}\left(\frac{2J_0(\alpha_i r/R)}{J_1(\alpha_i)\alpha_i}\right)\left(\frac{-4\cos((2n-1)\pi x/L)}{(-1)^n(2n-1)\pi}\right)e^{-\left(\frac{\alpha_i^2}{\alpha} + \frac{(2n-1)^2\pi^2}{\beta}\right)\frac{t}{\tau}} \quad [13]$$

where $\alpha = R^2/(R^2 + L^2)$, $\beta = L^2/(R^2 + L^2)$, $\tau = (R^2 + L^2)/\tilde{D}$, $J_0$ and $J_1$ the 0th and 1st order Bessel function, respectively, and $\alpha_i$ the $i$th zeroth of $J_0$. An expression for the decay current can be obtained by integrating the oxygen ion flux over the sample surface. Using Eq. 2 and 13, we find

$$I(t) = \Delta Q\left(\frac{32}{\alpha\beta\tau}\right)\sum_{i\in N^+}\sum_{n\in N^+}\left(\frac{\alpha}{\alpha_i^2} + \frac{\beta}{(2n-1)^2\pi^2}\right)e^{-\left(\frac{\alpha_i^2}{\alpha} + \frac{(2n-1)^2\pi^2}{\beta}\right)\frac{t}{\tau}} \quad [14]$$

where $\Delta Q$ is the charge involved in the equilibration process given by $\Delta Q = -2e\pi R^2 L(c_O^\infty - c_O^0)$. The current decay in the frequency domain, $\bar{I}(\omega)$, can be derived by Fourier transformation of Eq. 14. Fourier transformation of the step in the *EMF* leads to

$$\overline{EMF}(\omega) = \frac{\Delta EMF}{j\omega} \quad [15]$$

where $\Delta EMF$ is the magnitude of the potentiostatic step applied. Finally, the impedance is obtained by evaluating $Z(\omega) = \overline{EMF}\ (\omega)/I(\omega)$

$$Z(\omega) = \left(\frac{\partial EMF}{\partial Q}\right)\left(\frac{\alpha\beta\tau}{32}\right)\left(\sum_{i\in N^+}\sum_{n\in N^+}\left(\frac{\alpha}{\alpha_i^2} + \frac{\beta}{(2n-1)^2\pi^2}\right)\left(\frac{j\omega\tau}{j\omega\tau + \alpha_i^2/\alpha + (2n-1)^2\pi^2/\beta}\right)\right)^{-1} \quad [16]$$

where $(\Delta EMF/\Delta Q)$ has been replaced by the derivative of the $EMF$ with respect to $Q$. The latter replacement is allowed when the voltage step is small. When $R >> L$, Eq. 16 simplifies to the well-known expression corresponding to one-dimensional diffusion[12,13]

$$Z(\omega) = \left(\frac{\partial EMF}{\partial Q}\right)\frac{1}{j\omega}\sqrt{\frac{i\omega\tau'}{4}}\ \coth\left(\sqrt{\frac{j\omega\tau'}{4}}\right) \quad [17]$$

where $\tau' = L^2/\tilde{D}$

The above expressions for $Z(\omega)$ have been derived by solving Fick's second law under the boundary conditions characteristic for a potentiostatic step. It can be shown that any other set of boundary conditions leads to the same expression for $Z(\omega)$. Both expressions 16 and 17 lead to a $\omega^{-1/2}$ dependence of $Z$ at high frequencies. The latter dependence corresponds with semi-infinite diffusion and the corresponding diffusion element is referred to as the Warburg impedance. The Warburg impedance gives rise to a linear line with slope equal to 1 in the complex impedance plane.

## Experimental

*Sample preparation.*—$La_{0.8}Sr_{0.2}CoO_{3-\delta}$ powder was prepared by thermal decomposition of precursor complexes derived from nitrate solutions using ethylene-diaminetetraacetetic acid (EDTA) as a complexing agent.[14,15] The resulting powder was milled for several hours and calcined at 925°C in stagnant air for 10 h. Disks were obtained by uniaxially static pressing at 1.5 bar followed by isostatic pressing at 4000 bar. These disks were sintered at 1125°C for 10 h in air. The density of the resulting disks determined by an Archimedes method was typically 96 to 98% of the theoretical one (6.95 g/cm$^3$ [16]). Cylindrical samples were cut 7.75 mm in diam and 2 mm thick. Before measurements, these samples were polished with 1000 mesh SiC.

ZY13 ($Zr_{0.87}Y_{0.13}O_{1.935}$) solid electrolytes were prepared from Zircar commercial powder. These were uniaxially and isostatically pressed into pellets at the same pressure used for the perovskite samples. After sintering at 1400°C for 5 h, disks of appropriate dimensions were cut from these pellets.

*Experimental setup.*—Two different cell designs were used in this study. These are shown schematically in Fig. 1 and 2. In both cases a cylindrical disk of $La_{0.8}Sr_{0.2}CoO_{3-\delta}$ was placed in a cell with a small internal volume of approximately 280 mm$^3$.

In cell 1, a ZY13 solid electrolyte disk of 12 mm in diam and 1 mm thick was sealed on an $Al_2O_3$ cylindrical crucible using a Pyrex glass ring. The box was 9 mm in internal diameter, 12 mm in external diameter, and 4 mm in depth. Two Pt-based electrodes were painted on the inner side of the ZY13 disk using Pt-paste. These electrodes were connected to Pt wires outside the cell using a very thin Pt tape (0.05 mm). A single Pt-electrode was painted on the outer surface of the ZY13 disk.

Cell 2 differs from cell 1 in that the $Al_2O_3$ cylindrical crucible was replaced by a ZY13 crucible. In this arrangement, the ZY13 disk was used to measure the $EMF$ and the crucible to pump oxygen into or out of the cell. Pt-based electrodes were painted on opposite sides of both the disk and crucible, as indicated in Fig. 2. The inner electrodes

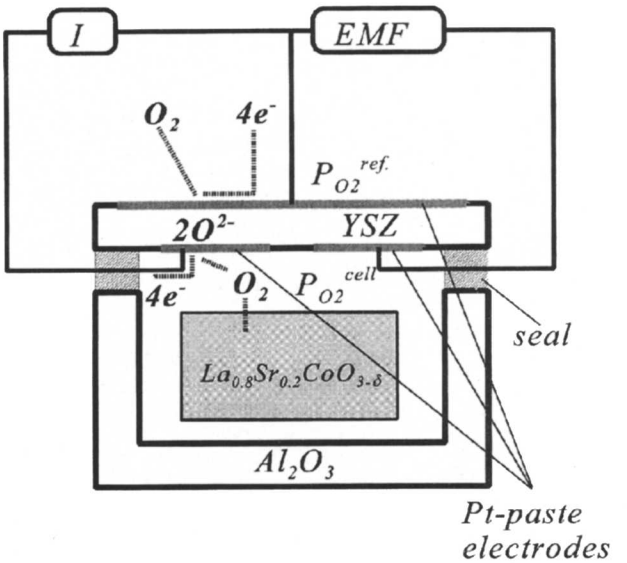


**Fig. 1. Schematic diagram of the electrochemical cell denoted as cell 1.**

were short-circuited by means of Pt-tape which was led to the exterior of the cell via the Pyrex glass seal. The cell dimensions were chosen similar to that of cell 1.

Preliminary experiments were performed with a cell similar to the one used by Gür and Beltzner,[9,10] which authors did not use an internal reference electrode. However, these measurements showed that polarization losses at the inner ZY13/Pt/$O_2$ interface changed too much during potentiostatic steps, so that no reliable data of oxygen diffusion could be obtained. The two cells in this study are similar to that used by Lade and Jacobsen[17] except for the fact that we applied a reference electrode to take into account the $P_{O_2}^{cell}$ dependent polarization losses at the internal YSZ/Pt/$O_2$ interface. The cell used by Lade and Jacobsen contained a reference electrode to account for

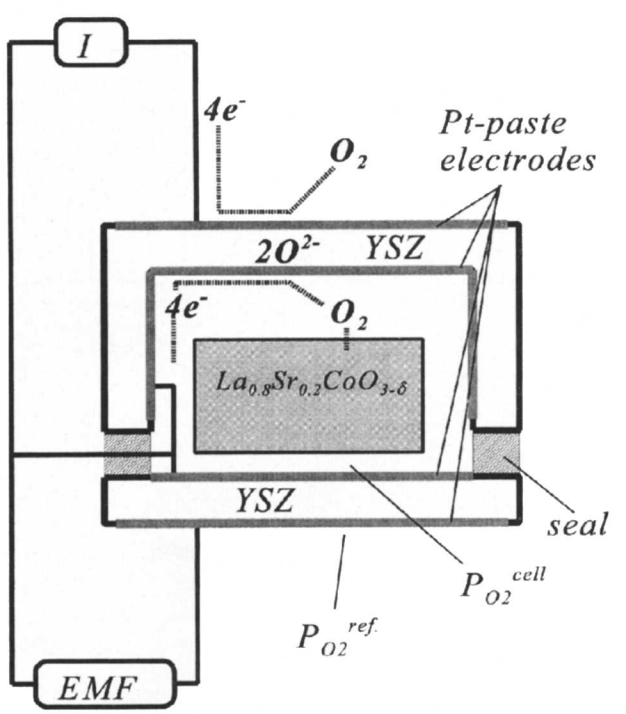


**Fig. 2. Schematic diagram of the electrochemical cell denoted as cell 2.**

the $P_{O_2}^{cell}$ independent polarization losses at the external YSZ/Pt/$O_2$ interface.

Both types of cells used in the present study were placed in a quartz tube used to flush the cell with air. Thermocouples to measure the temperature were positioned just below and above the cell. Potentiostatic steps were applied using a Solartron 1286 electrochemical interface. An HP 7500 series B data acquisition system was used to measure the cell *EMF* and current. Both apparatus were controlled with a computer.

*Potentiostatic step measurements.*—Potentiostatic steps of 25 mV were applied between 0 and 150 mV at 700, 800, 900, and 1000°C using cell 1 and at 750, 850, 950°C using cell 2. For clarity, a step of 25 mV corresponds to a change in the value of $\log(P_{O_2}^{cell})$ equal to 0.396 at 1000°C and equal to 0.518 at 700°C. The studied cell voltages thus correspond to an oxygen partial pressure range given by ($10^{-3.8}$ − 0.209 bar) at 700°C and ($10^{-3.1}$ − 0.209 bar) at 1000°C.

An external resistance of 2.4 Ω was placed in series with the cell in order to keep the maximum value of the decay current in the range permitted by the potentiostat.

*Data analysis.*—Experimental data of $I(t)$ were transformed to the frequency domain using the following procedure. Between successive data points, $I(t)$ was approximated by a second order polynomial function. The latter was obtained by least squares fitting, including three additional data points at either side. This polynomial function was Fourier transformed analytically and the results obtained for all pairs of successive data points were summed. The above procedure was used to evaluate $\bar{I}$ for 50 different values of the frequency. The corresponding values for $\overline{EMF}(\omega)$ were calculated using Eq. 15. The cell-impedance as a function of frequency was fitted to an equivalent circuit using the program EQUIVCRT.[12] The program was modified to incorporate the expression for finite-length diffusion of oxygen into a cylindrical sample, as given by Eq. 16. Details will be discussed elsewhere.[18]

## Results and Discussion

*Decay current and cell impedance.*—Decay currents measured at 800°C for several potentiostatic steps are shown in Fig. 3. It is seen that at long times after the step the decay currents decrease exponentially with time. The characteristic time corresponding to these exponential decays increases with decreasing $P_{O_2}$, which might be due to either an increase of the cell-resistance or a decrease in $\tilde{D}$. Transient current responses to a potentiostatic step from 0 to 25 mV at 700, 800, 900, and 1000°C are given in Fig. 4. A slope of −0.5 in the double logarithmic plots shown in these figures would correspond to the case of semi-infinite diffusion. The influence of the cell-resistance is clearly visible as a flattening of the curves at short times. Its importance to the decay current might explain discrepancies in the value of $\tilde{D}$ obtained from fitting experimental data of $I(t)$ either to the short or long time approximation.[9] In both these approximations, the transient current response is assumed to be purely diffusion controlled.

Impedance plots obtained from Fourier transformation of the decay currents (after a potentiostatic step from 0 to 25 mV) at various temperatures are shown in Fig. 5. All plots clearly show the typical curve of the coth-function (Eq. 17). Data could be fitted to an equivalent circuit consisting of a resistance, $R_{lump}$, in series with the element that describes the finite-length diffusion, $T$. A capacitance $C_{gas}$ was placed parallel to the diffusion element to fit the impedance data at high oxygen partial pressures. The latter is believed to be related with the capacity of the gas phase and its presence results in an increase of the slope (with the real axis) of the impedance at high frequencies. From the discussion in Appendix A, it is recognized that $C_{gas}$ will be a function of oxygen partial pressure in the cell. Its influence on the cell impedance is expected to be most severe at high oxygen partial pressure. Experimental values for $C_{gas}$ determined from the potentiostatic steps from 0 to 25 mV are shown in Table I. The values are reasonably close to the ones calculated from Eq. A-2. No accurate values for $C_{gas}$ could be obtained from measurements steps at low oxygen partial pressure.

The cell resistance $R_{lump}$ is assumed to be a lumped sum of various resistive contributions, including that of electrical wiring, gas-phase diffusion, and the resistance associated with limited oxygen transfer through the sample surface. It must be noted that, in principle, the equivalent circuit in which $C_{gas}$ is placed in series with $R_{lump}$ is not correct, since $C_{gas}$ should be placed parallel to the resistance associated with limited oxygen transfer through the sample surface. However, fitting the experimental impedance data at high $P_{O_2}$ to an equivalent circuit that included one resistance in parallel and one in series with $C_{gas}$ resulted in large scatter of the impedance parameters.

Values of $R_{lump}$ obtained from the reduction steps are given in Table II. The value of $R_{lump}$ is found to increase strongly with decreasing temperature and oxygen partial pressure. Therefore $R_{lump}$ also changed within a single step in the oxygen partial pressure. This effect is responsible for the limited accuracy of the values for $R_{lump}$ determined from the fitting-procedure. It is further seen from Table II that the total resistance of cell 2 was at all temperatures larger than that of cell 1. Recently performed experiments on other samples using cell 2 showed a much smaller cell-resistance than observed in this study using cell 2. This reduction of the resistance may be due to improved painting of the Pt layer on the inner sidewalls of the ZY13 crucible. The effect of this latter Pt layer is to increase the

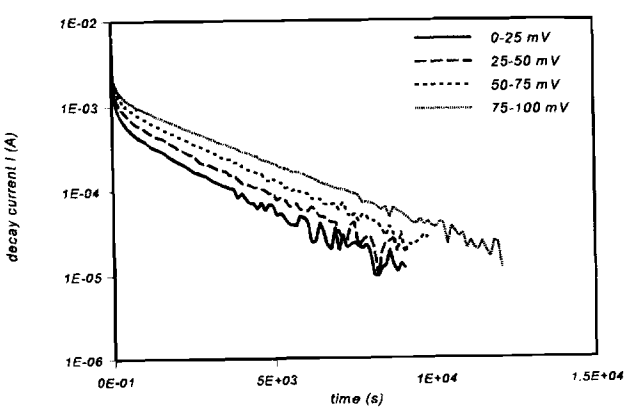


Fig. 3. Decay current vs. time in a single logarithmic plot. Curves represent transient current responses to potentiostatic steps of 25 mV in the range 0 to 100 mV at 800°C which were obtained using cell 1.

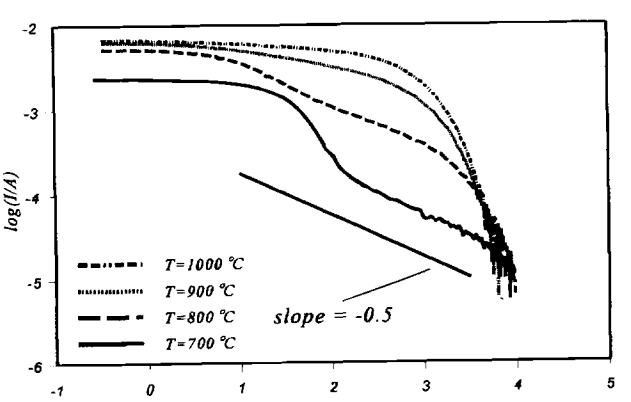


Fig. 4. Decay current vs. time in a double logarithmic plot. Curves represent transient current responses to potentiostatic steps from 0 to 25 mV which were obtained using cell 1.

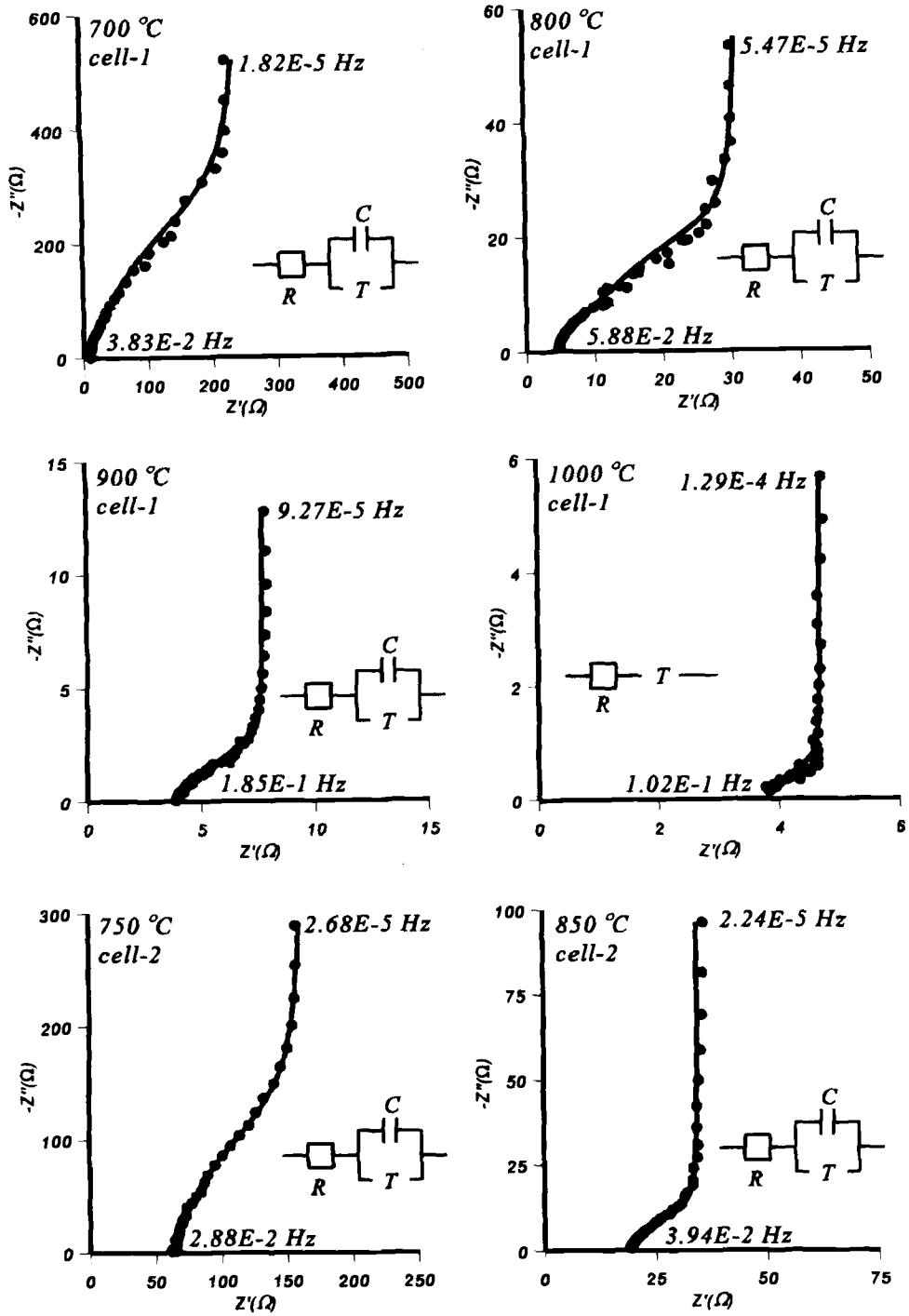


Fig. 5. Complex impedance representations from Fourier transformation of the decay current. Drawn lines indicate the best fit obtained with the equivalent circuit shown. The impedance data in these plots were not corrected for the external resistance of 2.4 Ω. The highest and lowest frequencies for which the impedance was calculated are also shown.

electrode area but also to decrease the effective gas-phase diffusion length, which should result in a corresponding decrease of the gas-phase diffusion resistance, $R_{gas}$. However, values of $R_{gas}$ calculated from Eq. B-3 are much smaller than experimentally observed values of $R_{lump}$. Furthermore, the latter values increase with decreasing temperature which is not expected from Eq. B-3. It can thus not be excluded that the total cell resistance is for a large part determined by limited oxygen transfer across the sample surface. In the latter case, the observed differ-

**Table I. Experimental values of the gas-phase capacitance as obtained from the impedance data of a potentiostatic step from 0 to 25 mV. Theoretical values calculated from Eq. A-2 using $V_{cell}$ = 190 mm³ are shown as well.**

| T (°C) | $C_{gas}^{exp}$ (F) | $C_{gas}^{the}$ (F) | Cell |
|---|---|---|---|
| 700 | 3.73 | 5.26 | 1 |
| 750 | 5.34 | 4.87 | 2 |
| 800 | 2.12 | 4.52 | 1 |
| 850 | 4.63 | 4.21 | 2 |
| 900 | 5.82 | 4.41 | 1 |

**Table II. Experimental values of $R_{lump}$ determined from the potentiostatic reduction steps. The values are corrected for an applied external resistance of 2.4 Ω.**

| | Cell 1 | | | Cell 2 | | | |
|---|---|---|---|---|---|---|---|
| | 950°C | 850°C | 750°C | 1000°C | 900°C | 800°C | 700°C |
| 0 to 25 mV | 13.2 | 19.1 | 63.1 | 1.3 | 1.5 | 2.3 | 8.3 |
| 25 to 50 mV | 14.1 | 20.9 | 63.1 | 1.3 | 1.5 | 2.3 | 9.1 |
| 50 to 75 mV | 16.6 | 24.5 | 70.8 | 1.3 | 1.6 | 2.6 | 9.2 |
| 75 to 100 mV | 19.9 | 30.9 | 95.5 | 1.6 | 1.6 | 2.9 | 9.9 |
| 100 to 125 mV | 33.1 | 42.7 | | 1.8 | 3.6 | 4.4 | 12.0 |
| 125 to 150 mV | | | | 2.9 | 6.0 | 6.8 | 17.8 |

ence in the resistance of cell 1 compared with that of cell 2 might result from differences in the surface structure or surface composition of the samples used.

*Oxygen diffusivity.*—Chemical diffusion coefficients obtained from reduction steps are always somewhat smaller than those from oxidation steps. This difference can be attributed to the nonlinear increase of the cell resistance $R_{lump}$ with decreasing oxygen partial pressure. For the same reason, no accurate diffusion coefficients could be determined at *EMF* values above 75 mV.

Average values of $\tilde{D}$ from reduction and oxidation steps as a function of temperature and oxygen partial pressure are given in Fig. 6. Good agreement is noted between the chemical diffusion coefficients obtained from both cells, in spite of their large difference in the value of the cell resistance $R_{lump}$.

Experimental data of oxygen nonstoichiometry, discussed in Part II of this paper, indicate a $P_{O_2}^{-\gamma}$ dependence of the oxygen vacancy concentration $c_V$ with $\gamma = 0.23$ at the conditions covered by our experiments. Substituting this proportionality into Eq. 6, we obtain the following relationship between $\tilde{D}$ and the vacancy diffusion coefficient, $D_V$

$$\tilde{D} = \frac{D_V}{2\gamma} \qquad [18]$$

Figure 6 shows that $\tilde{D}$ is almost independent of oxygen partial pressure which result confirms that $D_V$ is almost independent of oxygen vacancy concentration, as expected.

The Arrhenius plot of the chemical diffusivity is shown in Fig. 7. In this figure, data of $\tilde{D}$ were averaged over the

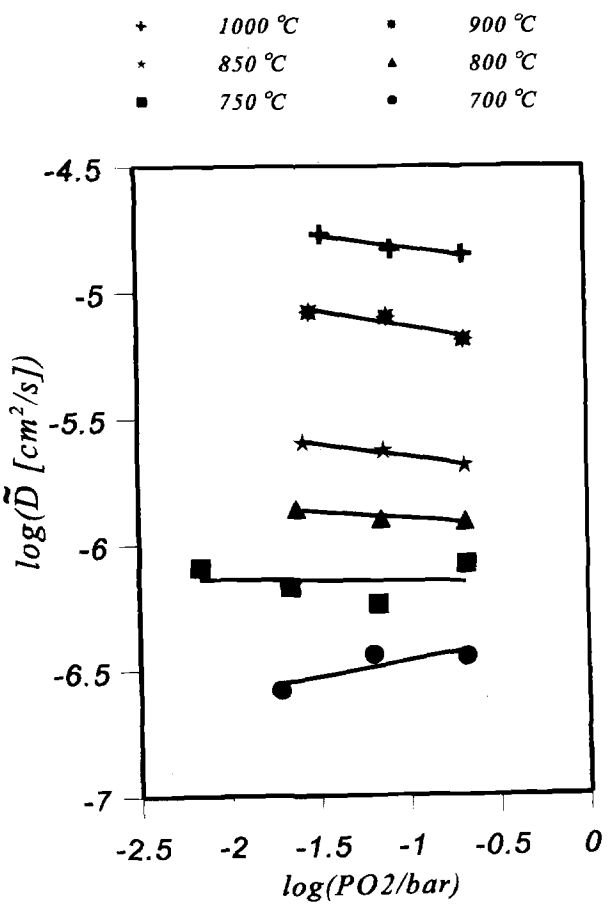


**Fig. 6. Chemical diffusion coefficient as a function of oxygen partial pressure measured at different temperatures. Both cell 1 and cell 2 were used for measurements. The oxygen partial pressures corresponding to the data points were calculated from the value of the *EMF* at the beginning of the potentiostatic step.**

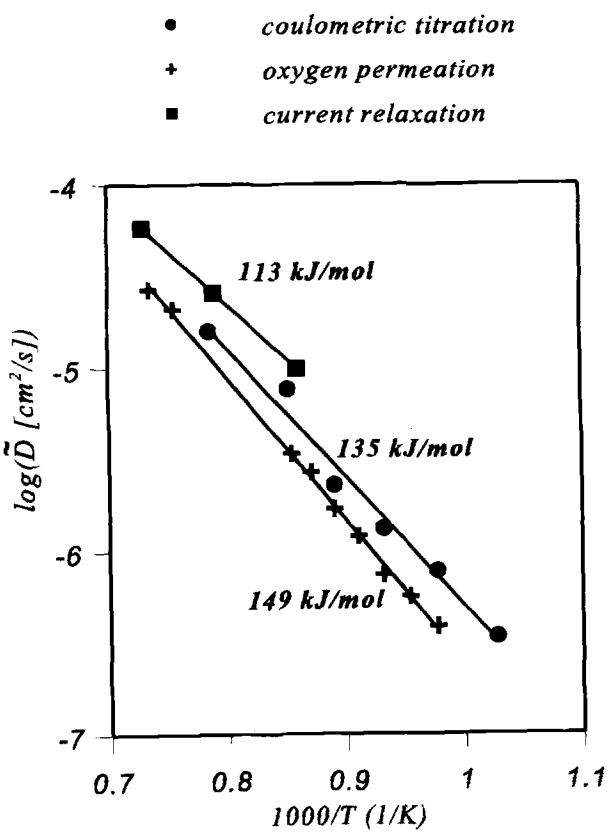


**Fig. 7. Arrhenius plot for the chemical diffusion coefficient. Data obtained from oxygen permeation[20] and current relaxation[19] experiments are shown for comparison.**

studied range in oxygen partial pressure. The activation energy is 135 ± 7 kJ/mol, which is in fair agreement with results calculated from electrical current relaxation[19] and oxygen permeation experiments.[20] The latter values were calculated as the ratio of the oxygen permeation flux with the vacancy concentration gradient applied. The vacancy concentration was calculated from the oxygen partial pressure using the oxygen nonstoichiometry model which will be introduced in Part II of this paper. The agreement found between the oxygen permeation and the chemical diffusion experiments, implies that all oxygen vacancies contribute to the total oxygen ion flux.

It follows that $\tilde{D}$ in $La_{0.8}Sr_{0.2}CoO_{3-\delta}$, can be represented as

$$\tilde{D}[cm^2/s] = 5.91 \times e^{\frac{-135\ kJ/mol}{RT}} \qquad [19]$$

The vacancy diffusion coefficient can be obtained from $D_V = 0.46 \times \tilde{D}$. Both $\tilde{D}$ and $D_V$ are almost independent of oxygen partial pressure. The oxygen self-diffusion coefficient can be calculated from Eq. 5, which results in

$$D_O[cm^2/s] = 2.72 \times \left(\frac{\delta}{3-\delta}\right) \times e^{\frac{-135\ kJ/mol}{RT}} \qquad [20]$$

It is recognized that $D_O$ is proportional to the nonstoichiometry parameter $\delta$, the value of which is a strong function of oxygen partial pressure and temperature.

## Conclusions

Direct Fourier transformation of the experimental decay current after a potentiostatic step yields impedance plots which show the coth-behavior expected for finite length diffusion. At low temperatures and high oxygen partial pressures, the influence of the gas-phase capacitance of the cell is seen in the high frequency part of the impedance plots.

Chemical diffusion coefficients were determined for $La_{0.8}Sr_{0.2}CoO_{3-\delta}$ as a function of oxygen partial pressure

and temperature. The value of $\tilde{D}$ is almost independent of oxygen partial pressure. The activation energy is equal to 135 ± 7 kJ/mol. The fair agreement noted between values of $\tilde{D}$ obtained from relaxation and oxygen permeation experiments strongly suggest that all oxygen vacancies contribute to oxygen ion transport in $La_{0.8}Sr_{0.2}CoO_{3-\delta}$. The combined data of $\tilde{D}$ and oxygen nonstoichiometry indicate that the vacancy diffusion coefficient is almost independent of oxygen partial pressure.

## Acknowledgments

A. Nijmeijer and H. Kruidhof are gratefully acknowledged for preparing the samples. The authors would like to thank B. van Hassel and G. Mollenhorst for their recommendations regarding the design of the electrochemical cell.

Manuscript submitted July 16, 1996; revised manuscript received Dec. 12, 1996.

*The Univeristy of Twente assisted in meeting the publication costs of this article.*

## APPENDIX A

### Gas-Phase Capacitance

The gas-phase capacitance is equal to the number of coulombs per unit change in *EMF* that must be electrochemically pumped in order to adjust the oxygen concentration of the gas phase to the imposed *EMF*

$$C_{gas} = 4F\frac{\Delta N_{O_2}^{gas}}{\Delta EMF} \qquad [A\text{-}1]$$

The *EMF* of the cell is given by the Nernst equation (Eq. 8). If we denote the initial value and value of the *EMF* after a potentiostatic step as $EMF_i$ and $EMF_f$, respectively, application of the ideal gas law leads to

$$C_{gas} = \left(\frac{4FV^{cell}P_{O_2}^{air}}{RT(EMF_i - EMF_f)}\right)\left(e^{\frac{-4FEMF_i}{RT}} - e^{\frac{-4FEMF_f}{RT}}\right) \qquad [A\text{-}2]$$

where $V^{cell}$ is the free internal volume of the cell (corrected for the volume of the sample).

## APPENDIX B

### Gas-Phase Diffusion Resistance

Theoretical values for the resistance $R_{gas}$ associated with molecular oxygen diffusion can be obtained from Fick's first law. Linearization across the effective thickness $\xi$ of the stagnant gas-phase layer, using the ideal gas law, yields

$$J_{O_2} = -D_{O_2}\frac{\Delta c_{O_2}}{\xi} = -D_{O_2}\frac{\Delta P_{O_2}}{RT\xi} \qquad [B\text{-}1]$$

where $D_{O_2}$ is the oxygen diffusion coefficient in the $O_2/N_2$ gas mixture inside the cell. From the expressions,[8] B-1, and $I = -4FAJ_{O_2}$, where $A$ is the area of the gas-phase diffusion layer, we obtain

$$R_{gas} = \left(\frac{RT}{4F}\right)^2\frac{\xi}{AD_{O_2}P_{O_2}} \qquad [B\text{-}2]$$

Substituting the appropriate expression for $D_{O_2}$ taken from Ref. 21 in Eq. B-2, and implementing the maximal values of the cell-dimensions, *i.e.*, $\xi < 5$ mm and $A > 17$ mm$^2$, leads to the following upper limit for $R_{gas}$

$$R_{gas}[m\Omega] \leq 6.8 \times \sqrt{\frac{T[K]}{1000}}\left(\frac{P_{N_2} + P_{O_2}}{P_{O_2}}\right) \qquad [B\text{-}3]$$

where $P_{N_2}$ is the pressure of the nitrogen gas inside the cell, the value of which in air is approximately 0.8 bar.

## REFERENCES

1. B. C. H. Steele, in *Mass Transport in Oxides*, J. B. Wachtman and A. D. Franklin, Editors, p. 165, National Bureau of Standards, Special Publication 296, Washington, DC (1968).
2. M. H. R. Lankhorst, H. J. M. Bouwmeester, and H. Verweij, *J. Am. Ceram. Soc.*, Submitted.
3. H. U. Anderson, C. C. Chen, L. W. Tai, and M. M. Nasrallah, in *Proceedings of 2nd International Symposium on Ionic and Mixed Conducting Ceramics*, T. A. Ramanarayanan, W. L. Worrell, and H. L. Tüller, Editors, PV 94-12, p. 376, The Electrochemical Society Proceedings Series, Pennington, NJ (1994).
4. H. J. M. Bouwmeester, H. Kruidhof, and A. J. Burggraaf, *Solid State Ionics*, **72,** 185, (1994).
5. M. H. R. Lankhorst and H. J. M. Bouwmeester, *This Journal*, **144,** 1268 (1997).
6. C. Wagner, *Z. Phys. Chem.*, **21,** 25, (1933).
7. M. H. R. Lankhorst, H. J. M. Bouwmeester, and H. Verweij, *J. Am. Ceram. Soc.*, Submitted.
8. W. Weppner and R. A. Huggins, *This Journal*, **24,** 1569 (1977).
9. T. M. Gür, A. Belzner, and R. A. Huggins, *J. Membrane Sci*, **75,** 151 (1992).
10. A. Belzner, T. M. Gür, and R. A. Huggins, *Solid State Ionics*, **57,** 327 (1992).
11. A. Honders and G. H. J. Broers, *ibid.*, **15,** 173, (1985).
12. B. A. Boukamp, *ibid.*, **20,** 31 (1986).
13. I. D. Raistrick and R. A. Huggins, *ibid.*, **7,** 213 (1982).
14. J. E. ten Elshof, H. J. M. Bouwmeester, and H. Verweij, *Appl. Catal. A: General*, **130,** 195 (1995).
15. R. H. E. van Doorn, H. Kruidhof, H. J. M. Bouwmeester, and A. J. Burggraaf, *J. Amer. Ceram. Soc.*, Submitted.
16. L. W. Tai, M. M. Nasrallah, H. U. Anderson, D. M. Sparlin, and S. R. Sehlin, *Solid State Ionics*, **76,** 295 (1995).
17. K. Lade and T. Jacobsen, *ibid.*, **72,** 218, (1994).
18. B. A. Boukamp and M. H. R. Lankhorst, *This Journal*, To be submitted.
19. Y. Denos, F. Morin, and G. Trudel, in *Proceedings 2nd International Symposium Ionic and Mixed Conducting Ceramics*, T. A. Ramanarayanan, W. L. Worrell, and H. L. Tüller, Editors, PV 94-12, p. 307, The Electrochemical Society Proceedings Series, Pennington, NJ (1994).
20. R. H. E. van Doorn, H. Kruidhof, H. J. M. Bouwmeester, and A. J. Burggraaf, *This Journal*, Submitted.
21. R. B. Bird, W. E. Stewart, and E. N. Lightfoot, *Transport Phenomena*, p. 508-513, John Wiley & Sons, Singapore (1960).